

Empirical ground-motion models for point- and extended-source crustal earthquake scenarios in Europe and the Middle East

S. Akkar · M. A. Sandikkaya · J. J. Bommer

Received: 19 December 2012 / Accepted: 30 May 2013 / Published online: 31 May 2013
© Springer Science+Business Media Dordrecht 2013

Abstract This article presents the latest generation of ground-motion models for the prediction of elastic response (pseudo-) spectral accelerations, as well as peak ground acceleration and velocity, derived using pan-European databases. The models present a number of novelties with respect to previous generations of models (Ambraseys et al. in *Earthq Eng Struct Dyn* 25:371–400, 1996, Bull Earthq Eng 3:1–53, 2005; Bommer et al. in Bull Earthq Eng 1:171–203, 2003; Akkar and Bommer in *Seismol Res Lett* 81:195–206, 2010), namely: inclusion of a nonlinear site amplification function that is a function of V_{S30} and reference peak ground acceleration on rock; extension of the magnitude range of applicability of the model down to M_w 4; extension of the distance range of applicability out to 200 km; extension to shorter and longer periods (down to 0.01 s and up to 4 s); and consistent models for both point-source (epicentral, R_{epi} , and hypocentral distance, R_{hyp}) and finite-fault (distance to the surface projection of the rupture, R_{JB}) distance metrics. In addition, data from more than 1.5 times as many earthquakes, compared to previous pan-European models, have been used, leading to regressions based on approximately twice as many records in total. The metadata of these records have been carefully compiled and reappraised in recent European projects. These improvements lead to more robust ground-motion prediction equations than have previously been published for shallow (focal depths less than 30 km) crustal earthquakes in Europe and the Middle East. We conclude with suggestions for the application of the equations to seismic hazard assessments in Europe and the Middle East within a logic-tree framework to capture epistemic uncertainty.

Electronic supplementary material The online version of this article (doi:10.1007/s10518-013-9461-4) contains supplementary material, which is available to authorized users.

S. Akkar (✉) · M. A. Sandikkaya
Department of Civil Engineering, Earthquake Engineering Research Center,
Middle East Technical University, K6 Building, 06800 Ankara, Turkey
e-mail: sakkar@metu.edu.tr

J. J. Bommer
Civil and Environmental Engineering, Imperial College London, London SW7 2AZ, UK

Keywords Ground-motion prediction equations · Seismic hazard assessment · Pan-European strong-motion database · 5 % acceleration spectral ordinates · PGA · PGV

1 Introduction

The evolution of strong ground-motion recording and modeling in Europe has always been some way behind that in the western United States. The first accelerogram recorded in Europe was obtained more than 30 years after the first strong-motion recordings from the 1933 Long Beach earthquake in California, and the first set of ground-motion prediction equations (GMPEs) for response spectral ordinates in Europe was derived about 20 years after the first models in the United States. With time, however, the gap has been gradually closing and in this article we present a set of new GMPEs derived from European and Middle Eastern strong-motion data for crustal earthquakes that are comparable with the equations produced by the PEER Center Next Generation of Attenuation (NGA) project (Power et al. 2008). The continuous development in the field of ground-motion modeling means that just as this study brings pan-European GMPEs in line with the NGA models—now referred to as the NGA-West models to distinguish that endeavor from the on-going NGA-East project to develop new GMPEs for the Central and Eastern United States—the NGA-West2 models are being presented (Bozorgnia et al. 2012). As discussed later, the question arises as to whether efforts will continue to close the gap or whether the move will now be towards global GMPEs for regions of shallow crustal earthquakes.

The article begins with a brief overview of the evolution of ground-motion models in Europe and the Middle East, highlighting the new features of the models presented herein. The strong-motion database is then described, followed by a description of the selection of the functional form for the models, including the selection and definition of explanatory variables. The article then presents the regressions to obtain the coefficients of the equations and the associated sigma values, after which the new predictions are explored for a number of scenarios, and also compared with previous models.

2 A new generation of European ground-motion models

The historical development of ground-motion recording and prediction for the pan-European region is recounted by Bommer et al. (2010). Globally, there are more GMPEs for peak ground acceleration (PGA) than for elastic response spectral accelerations (Douglas 2003, 2011), although GMPEs are now generally derived for spectral ordinates and PGA simultaneously. The first equations for response spectral ordinates using strong-motion records from across Europe and the Middle East were those of Ambraseys et al. (1996), and these have undergone a number of revisions and improvements, as summarized in Table 1. In parallel, recent GMPEs have been produced for individual European countries such as Greece, Italy and Turkey (e.g., Danciu and Tselentis 2007; Bindi et al. 2010; Akkar and Çağnan 2010), but the focus herein is exclusively on models derived for all seismically-active regions bordering the Mediterranean Sea and extending to the Middle East. This excludes those models derived for this region using indigenous datasets supplemented by recordings from other regions such as California and Japan (e.g., Berge-Thierry et al. 2003; Fukushima et al. 2003).

Table 1 summarizes the evolution of GMPEs for the prediction of spectral ordinates in Europe and the Middle East, and Table 2 lists key characteristics of the same equations. The models included are the following, together with the codes used to identify them in the tables:

Table 1 Evolution of GMPEs for spectral ordinates for Europe and the Middle East

GMPE Feature	ASB96	BDS03	Aetal05	Betal07	AB10	This study
Three site classes						
Style-of-faulting						
Within- and between-event variability						
Magnitude-dependent attenuation						
Nonlinear magnitude scaling						
Parallel model for PGV						
Explicit inclusion of V_{s30}						
Nonlinear site response						
Consistent models for point and extended sources						
Anelastic attenuation ^a						

Dark grey cells indicate an effect in final model. Light grey cells indicate an effect investigated but not retained in the final model either because not statistically significant or coefficients non-physical

^a It should be noted that the expression ‘anelastic attenuation’ is only strictly valid for GMPEs for Fourier amplitudes and not response spectral ordinates

Table 2 Characteristics of GMPEs for spectral ordinates for Europe and the Middle East; each model also includes an equation for PGA

GMPE feature	ASB96	BDS03	Aetal05	Betal07	AB10	This study
Number of earthquakes	157	157	135	289	131	221
Number of records	422	422	595	997	532	1041
Horizontal component	Larger	Larger	Larger	GM	GM	GM
Minimum response period (s)	0.10	0.10	0.05	0.05	0.05	0.01
Maximum response period (s)	2.0	2.0	2.5	0.5	3.0	4.0
Magnitude scale	M_s	M_s	M_w	M_w	M_w	M_w
Minimum magnitude	4.0	4.0	5.0	3.0	5.0	4.0
Maximum magnitude	7.9	7.9	7.6	7.6	7.6	7.6
Maximum distance (km)	260	260	99	100	99	200
Number of free coefficients	6	8	10	10	10	11

Number of earthquakes and records reported for spectral acceleration at 0.1 s. *GM* Geometric mean of the two horizontal components

ASB96—Ambraseys et al. (1996); BDS03—Bommer et al. (2003); Aetal05—Ambraseys et al. (2005); Betal07—Bommer et al. (2007); AB10—Akkar and Bommer (2010). The equations for spectral displacement ordinates by Akkar and Bommer (2007a) are not included because these were superseded by Akkar and Bommer (2010) but would have identical entries to the latter in Tables 1 and 2.

Table 2 does not include a row for the distance metric because all of these models have been based on Joyner-Boore distance, R_{JB} , which is the horizontal distance to the closest point on the surface projection of the fault rupture (Joyner and Boore 1981). A predictive model that is based on the closest distance to fault rupture, R_{rup} , is not developed because the current pan-European strong-motion databases lack sufficiently detailed information about most causative fault ruptures to allow determination of this distance metric for most events.

Following the suggestion of Bommer and Akkar (2012) that GMPEs should be derived in pairs, one based on a point-source measure for use with area sources (at least for area sources other than the host zone containing the site, for which the simulation of virtual faults

is an unnecessary computational effort) and another using an extended-source metric for fault sources, in this study additional models based on hypocentral distance, R_{hyp} , and on epicentral distance, R_{epi} , are also presented. The reason for providing equations in terms of both point-source distance metrics is that hypocentral distance is considered to be a better metric, not least because studies have shown that the hypocenter is often located close to regions of large slip (Mai et al. 2005; Manighetti et al. 2005). Additionally, in performing inversions to obtain equivalent stochastic parameters for empirical GMPEs, Scherbaum et al. (2006) found that regardless of the distance metric used in the GMPE, hypocentral distance frequently yielded the best results (in terms of minimized misfit) for the stochastic parameters. However, the use of GMPEs based on R_{hyp} for PSHA requires integration over the depth distributions—which should not be achieved through the addition of logic-tree branches with alternative depths (Bommer and Scherbaum 2008), although it is legitimate to have branches with alternative depth distributions—with the attendant onus to determine depth distributions and the consequent computational penalty. The use of an R_{epi} -based model can bypass these issues. Additionally, the model based on epicentral distance allows direct comparison with the R_{JB} model, which may offer some advantages, including assurance about the behavior of the point-source distance-based equations.

From Table 1, the evolution of the complexity of the models is immediately apparent. The Ambraseys et al. (1996) equations were of a rather simple functional form and in addition to linear dependence on surface-wave magnitude, M_s , and geometric spreading as a function of R_{JB} , the only other explanatory variable were two dummy variables representing the variations in ground motions amongst three site classes. These classes (rock, stiff soil and soft soil) were nominally defined in terms of ranges of 30 m shear-wave velocities, V_{S30} , but at the time the equations were derived shear-wave velocity measurements were available for very few European strong-motion accelerograph sites (e.g., Rey et al. 2002).

The equations derived by Bommer et al. (2003) used the same database, explanatory variables and functional form as Ambraseys et al. (1996), but added two additional terms as functions of dummy variables to include the influence of reverse, normal or strike-slip faulting. This model also presented separately the within-event and between-event components of the aleatory variability (Al Atik et al. 2010); although Ambraseys et al. (1996) used the two-stage regression approach of Joyner and Boore (1981), they only reported total sigma values.

The model of Ambraseys et al. (2005) represented a major advance in European ground-motion modeling, adopting a more complex functional form for the equation that included the magnitude-dependence of the geometric spreading. Table 2 also records other notable advances embodied in this GMPE, including the move to moment magnitude, M_w , (the preferred choice for state-of-the-art hazard assessments) instead of M_s , and, through careful processing of the accelerograms, an extension of the range of response periods for which predictive equations were derived. Another important advance, which may not be immediately apparent from the information in Table 2, is that the database used for this study was considerably improved with respect to that of Ambraseys et al. (1996), including having a much larger average number of records per event and more complete metadata (e.g., centroid moment tensors). Although the total number of records is not much larger, it must be noted that the minimum magnitude was larger: M_w 5, which corresponds to roughly M_s 4.8 using the M_s – M_w relation of Scordilis (2006), rather than M_s 4. Moreover, although the maximum magnitude and distance ranges covered by Ambraseys et al. (1996) appear impressive, they actually correspond to a single recording from a large earthquake; the maximum event covered by the remainder of the database was M_s 7.3. All but one of the records were obtained at distances of less than 200 km, and below M_s 6.5, only four accelerograms were recorded at distances beyond 100 km.

The [Bommer et al. \(2007\)](#) equations were derived only to explore the influence of the magnitude range in the database and were not intended for use in seismic hazard assessments (for which they would be hampered by the very limited period range that they cover). The GMPE of [Akkar and Bommer \(2010\)](#) was based on the same database as used by [Ambraseys et al. \(2005\)](#)¹, but the individual re-processing of all the records to determine the maximum usable period ([Akkar and Bommer 2006](#)), enabled the maximum response period to be extended to 3 s; this is still much shorter than would be desirable but is a consequence of the large proportion of the database obtained on analogue accelerographs. The functional form adopted for this equation was similar to that adopted by [Ambraseys et al. \(2005\)](#) but additionally included a quadratic term in magnitude. This model also included a model for peak ground velocity, PGV, which had previously been derived separately ([Akkar and Bommer 2007b](#)); this is noteworthy since although most engineering design applications make use of response spectra, there are a number of uses for PGV ([Bommer and Alarcón 2006](#)). As noted in Table 2, this study also adopted the more widely-used convention of the geometric mean of the horizontal components rather than the larger of the two.

The new models presented in this article constitute a new generation of predictive equations rather than an incremental development. As discussed in the next section, the database has continued to expand in size, but more importantly there have been very significant improvements regarding the metadata associated with the accelerograms. One particular benefit of this is that for the first time the pan-European models include V_{S30} explicitly as an explanatory variable rather than generic site classes. The new models also include the influence of non-linear soil response; in deriving a predictive equation for PGV, [Akkar and Bommer \(2007b\)](#) searched without success for empirical evidence for soil nonlinearity in European strong-motion data. In this respect the new equations represent a departure from purely empirical fitting, with the use of externally developed models to constrain the influence of nonlinear soil response.

Another development envisaged regarding the functional form is the inclusion of an anelastic attenuation term to accommodate extrapolation of the equations beyond the 200 km limit of the dataset, which is almost inevitable in probabilistic seismic hazard analysis (PSHA). In passing we note that the use of the term ‘anelastic attenuation’ is not strictly correct since it applies to Fourier amplitude spectra (FAS) rather than response spectra, but the terms in GMPEs involving $\ln(R)$ and R are modeled after the geometric spreading and apparent attenuation (scattering plus anelastic) of FAS. However, it is noted that in almost all cases the coefficients on this term were found to be positive, so none of the final equations includes this effect. As noted in Table 1, two previous European GMPEs explored the inclusion of such terms but their authors also omitted them from the final models, suggesting that the European dataset is not currently sufficient to constrain both contributions to the decay of amplitude with distance, at least with a constant geometrical spreading model and not accounting for the Moho bounce effect. It may be the case that data recorded over a much wider range of distances would be needed to constrain such terms in the predictive models.

The derivation of these new equations also addresses a problem identified by [Bommer et al. \(2007\)](#), namely that empirical GMPEs, even if their functional form includes non-linear magnitude scaling, tend to over-estimate ground-motion amplitudes at the lower limit of their magnitude range. This observation has been subsequently confirmed for the NGA models by [Atkinson and Morrison \(2009\)](#) and [Chiou et al. \(2010\)](#). [Douglas and Jousset \(2011\)](#) discuss the reasons for this over-estimation using stochastic models. The new

¹ 63 records used by [Ambraseys et al. \(2005\)](#) were not available in unprocessed form so they were not used by [Akkar and Bommer \(2010\)](#).

models address this issue by extending the lower magnitude limit of the dataset to M_w 4. This means that when the models are applied at M_w 5 (often the lower end of integration within PSHA) they should not over-predict ground motions, unlike GMPEs that only use data down to M_w 5. We emphasize that the original motivation was not to provide models that can be used with confidence at M_w 4, but rather to remove the bias in the models at the commonly used lower limit of M_w 5 in PSHA, following the recommendation by [Bommer et al. \(2007\)](#) to include data to one magnitude unit lower than the minimum threshold in PSHA integrations. However, we conclude that the new models can be used for magnitudes as small as M_w 4.

Another innovation in these new equations is the extension of the range of periods at the shorter end, following new insights into the relatively low sensitivity of short-period ordinates to the high-frequency filtering of accelerograms ([Douglas and Boore 2011](#); [Akkar et al. 2011](#)). [Bommer et al. \(2012\)](#) provided coefficients at short periods as an extension of the model of [Akkar and Bommer \(2010\)](#), as well as exploring the options for interpolating missing coefficients at short periods; the new models presented in this article include 62 spectral ordinates starting from the period of 0.01 s. The models presented here are reliable for structural periods up to 4 s, a longer period than previous generations of GMPEs for this part of the world (Table 2)².

3 Strong-motion database

The database compiled for this study is a subset of Reference Database for Seismic Ground-Motion in Europe (RESORCE) developed for the Seismic Ground Motion Assessment (SIGMA) project ([Akkar et al. 2013](#)). The databank is the extended and updated version of the pan-European strong-motion databases compiled under the Seismic Harmonization in Europe (SHARE) project ([Yenier et al. 2010](#)). In this study our database consists only of records from those stations with measured V_{S30} . The majority of stations have V_{S30} values that classify them as Eurocode 8 ([Comité Européen de Normalisation 2004](#)) classes B and C sites, i.e. $V_{S30} \leq 800$ m/s. There are few rock stations ($V_{S30} > 800$ m/s) classified based on measured V_{S30} values in the database. This is similar to the NGA database compiled by [Chiou et al. \(2008\)](#) and the majority of strong-motion databases worldwide.

When deriving the NGA GMPEs the developer teams accounted for possible differences in ground motions from main shocks and aftershocks by either excluding data from aftershocks or by including terms to model these differences, which for short-period motions were found to be up to 40 %. [Douglas and Halldórsson \(2010\)](#) investigated differences between spectral accelerations from main shocks and aftershocks using the same data as [Ambraseys et al. \(2005\)](#) but did not find any significant differences. Various damaging earthquakes in Europe that have been well recorded by strong-motion networks occurred as a series of events of similar magnitudes occurring on adjacent faults (e.g., Friuli 1976, Umbria-Marche 1997–1998, Molise 2002), which complicates the classification of earthquakes into main shocks and aftershocks. Due to these reasons, and the fact that up to half of the records available for this study come from earthquakes that could be classified as aftershocks, we have decided to retain all available strong-motion data for the derivation of the GMPEs. Any possible difference between aftershock and main shock motions is accommodated by the sigma value.

² [Akkar and Bommer \(2007a\)](#) provide coefficients up to 4 s but later [Akkar and Bommer \(2010\)](#) highlighted the unreliability of this model beyond 3 s because of a sharp reduction in the number of records used.

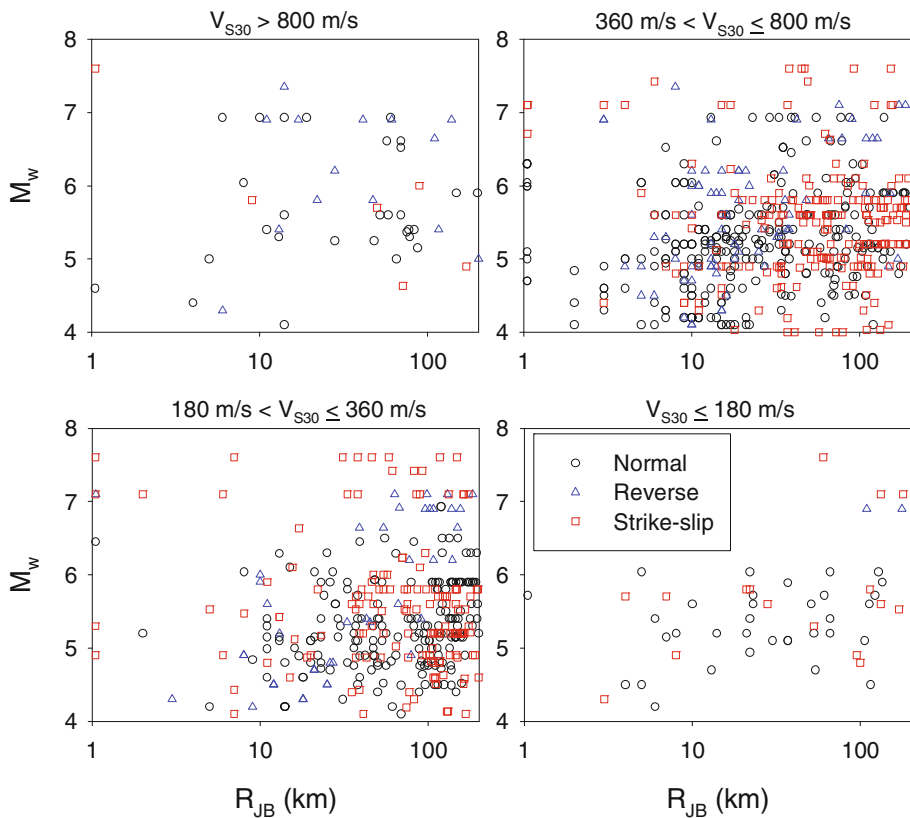
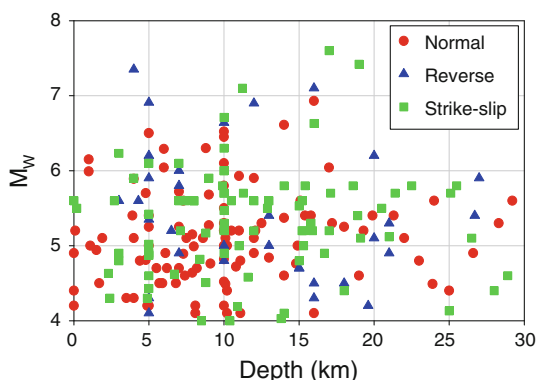


Fig. 1 Distribution of the data used in terms of magnitude, distance (R_{JB}), style-of-faulting and Eurocode 8 site class.

The vast majority of data that are the basis of this study were obtained from strong-motion instruments triggered by accelerations higher than a pre-defined threshold. Consequently ground motions below this threshold are not recorded. This leads to preferential recording of only larger-than-average motions from small earthquakes and/or at large distances. If these data were included within the regression analysis then the derived GMPEs would be biased upwards for weak motions. Based on a preliminary investigation using the PGAs predicted by the GMPE of [Bommer et al. \(2007\)](#) and various instrument resolutions, it was concluded that the available data are roughly unbiased for $M_w > 4$ at distances up to 200 km (Dr. John Douglas, *personal communication*, 2011). Singly-recorded earthquakes from 163 events were removed from the ground-motion database in order not to inflate the estimate of between-event variability in the proposed GMPEs. We considered 3-component accelerograms (two horizontal and one vertical) in our final database to develop a vertical-to-horizontal spectral acceleration ratio model that replaces the model of [Bommer et al. \(2011\)](#) and is consistent with the GMPEs proposed here. The latter GMPE is presented in a companion article published in this issue ([Sandikkaya et al. 2013b](#)).

The distribution of the final database in terms of magnitude, source-to-site distance, style-of-faulting and Eurocode 8 site class is presented in Fig. 1. The distance measure is chosen as R_{JB} in the scatter plots as the use of R_{epi} or R_{hyp} does not significantly change the general picture displayed in this figure. From these scatter plots it can be seen that magnitudes up

Fig. 2 Distribution of the earthquakes with respect to magnitude, style-of-faulting and focal depth.



to roughly M_w 7 are well represented, particularly for normal and strike-slip faulting. For larger magnitudes there are almost no records from normal and reverse-faulting events and the available data are mainly from three large strike-slip earthquakes (Manjil, Kocaeli and Düzce). Reverse-faulting earthquakes are quite poorly represented whereas most data come from normal events: this is in contrast to the NGA models for which reverse earthquakes contribute a large proportion of the database and normal events relatively little. This prompts us to suggest that these new pan-European models should perhaps be considered in seismic hazard studies in the Basin and Range Province of the US where normal-faulting earthquakes dominate, in the same way that Spudich et al. (1999) developed a model based on global data for application in that region. The distribution with respect to style-of-faulting of the database for the current study is in part the consequence of using only records from sites with directly measured V_{S30} values, which excludes, for example, recordings from several large-magnitude earthquakes in Iran. The vast majority of earthquakes with $M_w > 6$ have focal depths less than 20 km whereas the depth distribution of events smaller than M_w 6 is roughly uniform between 0 and 30 km (Fig. 2). All earthquakes are shallower than 30 km; as with earlier European GMPEs, records from deeper events have been excluded from the database. A table summarizing our database is given in the Electronic Supplement to this article.

The individual filtering of each record means that the number of spectral accelerations available for regression at each period varies. The high-pass filtering effect on long-period spectral ordinates is minimized by applying the criteria given in Akkar and Bommer (2006). The number of records starts reducing for $T > 1$ s as the effect of the chosen high-pass filter values becomes more and more apparent. By 4 s about 60 % of the records in the database are still available for regression analysis. The available data decays rapidly after $T = 4$ s, which prevented going beyond this spectral period in the regressions. This rapid drop-off is due to a large proportion of records from analogue instruments within the databank used despite the conversion of most European strong-motion networks to digital accelerometers in the past decade. The Akkar et al. (2011) criteria to account for low-pass filtering effects on the short period spectral ordinates ($T < 0.05$ s) were not followed as its application did not result in significant changes in the total number of data in this period range.

The GMPEs are derived from pseudo-spectral accelerations for 5 % of critical damping for the geometric mean of the two horizontal components computed from the selected records. A predictive model that scales the 5 % damped spectral ordinates of the proposed GMPEs for different damping levels ranging between 1 and 30 % is presented in a companion paper in this issue (Sandikkaya et al. 2013b).

4 Functional form of predictive equations and regressions

To find an appropriate functional form that models the observed scaling in terms of magnitude, distance and style-of-faulting, we undertook many trial regressions, using the random-effects procedure of [Abrahamson and Youngs \(1992\)](#). These regressions were performed on the observed spectral accelerations at a handful of periods, adjusted to a constant V_{S30} of 750 m/s using the nonlinear site amplification model developed by [Sandikkaya et al. \(2013\)](#), which is the first site amplification model developed explicitly for pan-European sites. We also undertook some regressions using simple site classes to check the impact of adopting the [Sandikkaya et al. \(2013\)](#) site response model and similar scaling in terms of magnitude, distance and style-of-faulting was obtained. The following paragraphs first discuss the development of reference ground-motion model that addresses the magnitude, distance and style-of-faulting scaling of ground-motion amplitudes anchored at $V_{S30} = 750$ m/s (reference rock). The rest of the section introduces the complete model that modifies the reference rock motion estimations for different site conditions.

The optimum magnitude scaling expression for the proposed GMPE was obtained by analyzing the behavior of three main functional forms. The simplest model among these alternatives is the continuous quadratic magnitude scaling (designated as “Quadratic” herein) that is used in the [Akkar and Bommer \(2010\)](#) GMPE. This functional form is modified by adding a cubic magnitude term (abbreviated herein as “Cubic”) because [Douglas and Jousset \(2011\)](#) suggest that cubic magnitude scaling better represents the magnitude-dependent variation of ground motions for both small and large events (Figs. 2, 3 in their paper). As for the third alternative, we adopted the magnitude scaling proposed by [Abrahamson and Silva \(2008\)](#) and also by [Boore and Atkinson \(2008\)](#). This quadratic functional form (Q-hinged) introduces a hinging magnitude to the magnitude scaling to simulate magnitude saturation for events larger than this magnitude level. The efficiency of these alternative models is assessed by visual comparisons with the actual data trend (physical argument) and studying the reduction in between-event sigma. Our observations indicated that the impact of different functional forms on the between-event sigmas was minimal. Thus, we used the physical argument to decide on the final functional form in terms of magnitude scaling.

Figure 3 shows the comparisons of three magnitude scaling functions for PGA as well as spectral ordinates at $T = 0.2$ s, $T = 1$ s and $T = 4$ s. The observed data used in the comparisons are adjusted to a strike-slip rupture mechanism, $R_{JB} = 10$ km and reference rock site of $V_{S30} = 750$ m/s. The adjustment, or normalization, of the empirical data was done by developing individual GMPEs for each magnitude scaling function for the above spectral quantities. The [Sandikkaya et al. \(2013\)](#) site response model is used to scale the ground motions to reference rock conditions. The resulting reference rock empirical data trends from each one of these specific GMPEs do not show significant differences; the empirical data given in Fig. 3 are those obtained from the ground-motion model that uses Q-hinged magnitude scaling. As inferred from Fig. 3, all three functional forms exhibit similar scaling for magnitudes up to $M_w 6$ for all considered spectral ordinates. The negligible differences in these alternative functional forms for smaller magnitudes become significant after $M_w 7$. The quadratic magnitude scaling yields larger estimations with respect to the other two functional forms for $M_w \geq 7$. The functional form that includes a cubic magnitude term shows over-saturation (a decrease in ground-motion amplitudes with increasing magnitude) for $M_w \geq 7.25$. Although a cubic magnitude term is supported by predictions from stochastic models ([Douglas and Jousset 2011](#)), the empirical data do not reveal the existence of such over-saturation. The superior consistency between the Q-hinged functional form and the empirical data at large magnitudes

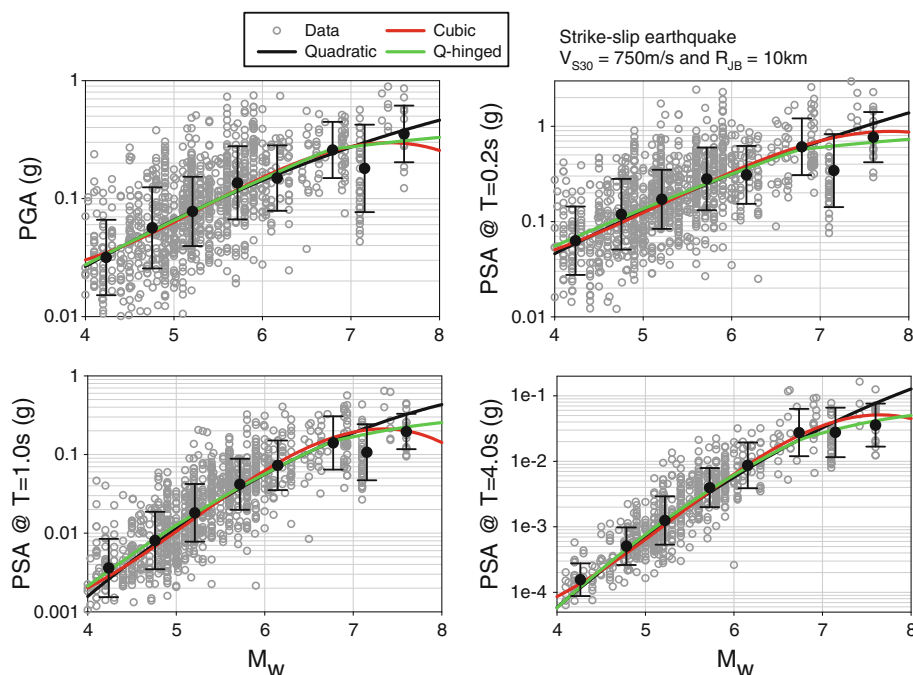


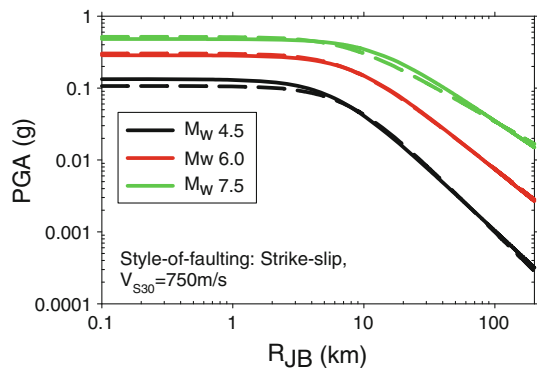
Fig. 3 Comparisons of magnitude-scaling trial functions with the empirical data for four spectral ordinates (PGA, PSA at $T = 0.2, 1.0$ and 4.0 s). The empirical data is calibrated for $R_{JB} = 10$ km, strike-slip rupture mechanism and $V_{S30} = 750$ m/s.

led us to prefer Q-hinged magnitude scaling in our final ground-motion model. However, we note that this might be somewhat unconservative and clearly there is greater epistemic uncertainty regarding the amplitudes at these larger magnitudes. Since the data do not reject any of the three models, a defensible course of action when applying the new equations proposed herein would be to add logic-tree branches with alternative higher and lower amplitudes for magnitudes of M_w 7.5 and larger, following a scheme such as that used by the USGS for the 2008 national hazard maps in the United States (Petersen et al. 2008).

The distance scaling of ground-motion amplitudes is studied separately for anelastic attenuation and the influence of magnitude-dependent distance saturation. Inclusion of the anelastic attenuation term yielded a positive regression coefficient, which is not justifiable as it implies an increase in ground-motion amplitudes with increasing distance. Two previous pan-European GMPEs (Ambraseys et al. 1996, 2005) that are listed in Table 1 also explored the possibility of including the anelastic attenuation term in their functional forms. Their analyses also did not converge to a physically meaningful result in terms of anelastic attenuation, as in our case. Thus, we removed the anelastic attenuation term from the final model. The magnitude-dependent distance saturation is accounted for by modifying the fictitious depth term with a multiplicative exponential term that is a function of magnitude. Figure 4 shows the distance scaling with and without magnitude-dependent distance saturation term.

The regression analysis resulted in very similar ground-motion estimations. The magnitude-dependent distance saturation slightly changes the median ground-motion

Fig. 4 Comparisons of magnitude-dependent and-independent distance saturation at different magnitudes for strike-slip style-of-faulting and a rock site of $V_{S30} = 750$ m/s. *Solid and dashed lines represent with and without magnitude-dependent distance saturation, respectively.*



estimations at short distances and towards intermediate distances for high magnitude events ($M_w 7.5$). Inclusion of magnitude-dependent distance saturation term also did not show a significant impact on the reduction of standard deviation. Therefore, we disregarded this term in the final ground-motion model to preserve the optimum number of estimator parameters in the prediction of ground motions. The observations on distance-scaling suggest that pan-European strong-motion databases still need supplementary recordings from wider distance ranges to allow simultaneous derivation of ‘geometric’ and ‘anelastic’ decay coefficients (these adjectives, as noted earlier, strictly only apply for Fourier amplitudes).

The style-of-faulting effect is addressed through multiplicative coefficients on dummy variables (additive in log space) in the reference model. We did not incorporate the depth effect while modeling different styles-of-faulting in our predictive model as the availability of depth-to-top-of-rupture information is very limited in the compiled strong-motion database. This metadata information might have been estimated through empirical relationships (e.g., Wells and Coppersmith 1994) but we avoided this option in order not to inflate the aleatory variability in ground-motion estimations. The style-of-faulting (SoF) is not uniformly distributed within the magnitude and distance range covered by the strong-motion database. For this reason, we trimmed the database by removing small-magnitude events ($M_w < 5$) having less than three recordings to obtain more accurate normal-to-strike-slip and reverse-to-strike-slip spectral amplitude ratios in order to prevent unexpected SoF scaling factors dominated by low-magnitude recordings. Style-of-faulting coefficients computed for three models using different distance metrics did not show significant differences along the period band of interest. This observation is counter to the findings of Bommer and Akkar (2012) for reverse-to-strike-slip (R:SS) ratios as their R:SS estimations from an R_{epi} -based model are higher than those predicted by a R_{JB} -based GMPE, although both ground-motion models were derived from the same database. This observation is attributed to the specific database features by Bommer and Akkar (2012) that are also discussed in the following section while we compare our style-of-faulting ratios with the estimations of other GMPEs. In essence, the proposed GMPEs of this study use the same style-of-faulting coefficients for all three models after smoothing those found for the three individual models based on different distance metrics, as suggested by Bommer and Akkar (2012).

The final functional form of our ground-motion predictive model is given in Eqs. (1)–(3):

$$\ln(Y) = \ln[Y_{REF}(M_w, R, SoF)] + \ln[S(V_{s30}, PGA_{REF})] + \varepsilon\sigma \quad (1)$$

where

$$\ln(Y_{REF}) = \begin{cases} a_1 + a_2(M_w - c_1) + a_3(8.5 - M_w)^2 + [a_4 + a_5(M_w - c_1)] \ln(\sqrt{R^2 + a_6^2}) + a_8 F_N + a_9 F_R + S & \text{for } M_w \leq c_1 \\ a_1 + a_7(M_w - c_1) + a_3(8.5 - M_w)^2 + [a_4 + a_5(M_w - c_1)] \ln(\sqrt{R^2 + a_6^2}) + a_8 F_N + a_9 F_R + S & \text{for } M_w > c_1 \end{cases} \quad (2)$$

and

$$\ln(S) = \begin{cases} b_1 \ln(V_{S30}/V_{REF}) + b_2 \ln \left[\frac{PGA_{REF} + c(V_{S30}/V_{REF})^n}{(PGA_{REF} + c)(V_{S30}/V_{REF})^n} \right] & \text{for } V_{S30} \leq V_{REF} \\ b_1 \ln \left[\frac{\min(V_{S30}, V_{CON})}{V_{REF}} \right] & \text{for } V_{S30} > V_{REF} \end{cases} \quad (3)$$

Equations (1)–(3) indicate that the median spectral acceleration $\ln(Y)$ is computed by modifying the reference ground-motion model $\ln(Y_{REF})$ through the nonlinear site amplification function $\ln(S)$. The estimator parameters of the reference ground-motion model are as follows: moment magnitude, M_w ; source-to-site distance measure, R (km), for which R_{JB} , R_{epi} , R_{hyp} are used for different models; and the style-of-faulting dummy variables, F_N and F_R that are unity for normal and reverse faults, respectively, and zero otherwise. The parameter c_1 in the reference ground-motion model is the hinging magnitude and it is not obtained as part of regression analysis. It is taken as M_w 6.75 (which happens to be the same value used in [Boore and Atkinson 2008](#)) and is imposed in the regression analysis after making several observations in the empirical data trend for different magnitude and distance interval. The total aleatory variability of the model is given by σ that is composed of within-event (ϕ) and between-event (τ) standard deviations (SDs). The period-dependent estimators parameters of the nonlinear site function (i.e., b_1 and b_2) as well as the period-independent c and n coefficients are directly adopted from the [Sandikkaya et al. \(2013\)](#) model. The reference V_{S30} (V_{REF}) is 750 m/s in the nonlinear site model and $V_{CON} = 1,000$ m/s that stands for the limiting V_{S30} after which the site amplification is constant. The reference rock site PGA (PGA_{REF}) is calculated from the reference ground-motion model in Eq. (2). It is the updated version of PGA_{REF} model given in [Sandikkaya et al. \(2013\)](#) by considering the particular magnitude, distance and style-of-faulting distributions of the strong-motion database used in this study. Regressions were performed by first scaling observed spectral ordinates to reference rock conditions. The units of pseudo-spectral acceleration and PGA are in terms of gravitational acceleration g whereas PGV is in units of cm/s in Eqs. (2) and (3).

No smoothing or truncation is done on the regression coefficients due to the unexpected jagged variation of response spectrum estimations observed in the [Akkar and Bommer \(2007a,b\)](#) predictive model. This problem is discussed in detail by [Akkar and Bommer \(2010\)](#) and it was one of the motivations behind the development of the new GMPE in that paper, which superseded the former [Akkar and Bommer \(2007a,b\)](#) model. The fictitious depth coefficient (a_6) was decided to be kept with one decimal as trials in regressions showed that the increase in its precision neither improves the ground-motion predictions nor decreases the SD of the model. The period independence of this coefficient stems from the observations made from many trials in regression analysis as variations in a_6 were found to be minimal in the spectral period band of interest in our model. A similar observation on the behavior of this coefficient was also observed in [Bommer et al. \(2011\)](#) that describe the recent pan-European vertical-to-horizontal spectral ratio model. A similar reasoning also applies to the linear magnitude coefficients (i.e., a_2 , a_5 and a_7) as they do not show significant

Table 3 Period-independent regression coefficients

a_2	a_5	a_6	a_7	c_1	c	n
0.0029	0.2529	7.5	−0.5096	6.75	2.5	3.2

fluctuations across the spectral period band of interest: we constrained them to the regression coefficients computed for PGA for the models using R_{JB} , R_{epi} and R_{hyp} . Keeping these coefficients as constants also resulted in a smooth variation of period-dependent spectral ordinate estimations for the entire ranges of period, magnitude and distance covered by the proposed models. Table 3 lists the period-independent coefficients of the proposed models. Table 4 presents the period-dependent coefficients, and between- and within-event SDs for some selected periods. Both Tables 3 and 4 contain the coefficients of nonlinear site model for completeness. The full list of the regression coefficients of the proposed ground-motion models for all three distance measures are given in the Electronic Supplement to this article. The Electronic Supplement also includes a Matlab script, its sample input and an Excel macro to compute the spectral ordinates from the proposed models for different earthquake scenarios.

As a check on the statistical behavior of the developed models, Fig. 5 presents residual plots for spectral ordinates at three response periods with respect to M_w , R and V_{S30} for the model using R_{JB} (residual plots for the other models are similar). The residuals are grouped into several magnitude, distance and V_{S30} bins to show the average residual variation (solid circles on each plot) for each independent variable. The error bars given on the same plots indicate the ± 1 SD about the bin averages. The within-event residuals as a function of distance do not show any apparent trends. The proposed model slightly overestimates motion at very soft soil sites ($V_{S30} < 180$ m/s) and underestimates motions for rock sites ($V_{S30} > 800$ m/s) at relatively short periods ($T = 0.2$ s). This observation, however, may not reflect the actual performance of the ground-motion model as the data in these V_{S30} ranges are sparse and poorly distributed. The magnitude-dependent variation of between-event residuals also suggests some level of bias towards large magnitudes at all periods. The between-event residuals appear to show a narrowing at all periods with increasing magnitude up to M_w 7, which could suggest a reduction of aleatory variability at large magnitudes. However, the sampling of data at large magnitudes is sparse and this could be the cause of the apparently smaller variability and the observed bias (particularly at $T = 1$ s). In two previous sets of GMPEs for Europe and the Middle East (Ambraseys et al. 2005; Akkar and Bommer 2007a) such behavior led to the characterization of sigma as linearly dependent on magnitude. Later on it was argued (Akkar and Bommer 2010) that the appearance of a magnitude-dependent sigma could be because data are only available from a handful of large-magnitude earthquakes leading to an underestimation of the true variability at $M_w > 6.5$, and because of poorly constrained metadata (particularly seismic moments) for smaller events, which despite the improvements in the current database is a problem that is likely to still persist to some degree. We think that these arguments still hold and we do not model the SD as a function of magnitude in the current set of GMPEs.

Figure 6 shows the period-dependent variation of the between-event, within-event and total sigmas for the GMPEs derived in this study. As is universally observed, within-event sigmas are much larger than the between-event component (e.g., Strasser et al. 2009). The between-event variability is almost model-independent but the within-event variability of the R_{JB} model is slightly lower than the other two GMPEs, as would be expected. The SDs

Table 4 Period-dependent regression coefficients of the (a) R_{JB} , (b) R_{epi} , (c) R_{hyp} ground-motion model

Period(s)	a_1	a_3	a_4	a_8	a_9	b_1	b_2	ϕ	τ	σ
(a)										
PGA	1.85329	-0.02807	-1.23452	-0.1091	0.0937	-0.41997	-0.28846	0.6201	0.3501	0.7121
0.01	1.87032	-0.0274	-1.23698	-0.1115	0.0953	-0.41729	-0.28685	0.6215	0.3526	0.7146
0.02	1.95279	-0.02715	-1.25363	-0.104	0.1029	-0.39998	-0.28241	0.6266	0.3555	0.7204
0.03	2.07006	-0.02403	-1.27525	-0.0973	0.1148	-0.34799	-0.26842	0.641	0.3565	0.7335
0.04	2.20452	-0.01797	-1.30123	-0.0884	0.1073	-0.27572	-0.24759	0.6534	0.3484	0.7405
0.05	2.35413	-0.01248	-1.32632	-0.0853	0.1052	-0.21231	-0.22385	0.6622	0.3551	0.7514
0.075	2.63078	-0.00532	-1.35722	-0.0779	0.0837	-0.14427	-0.17525	0.6626	0.3759	0.7618
0.10	2.85412	-0.00925	-1.38182	-0.0749	0.0761	-0.27064	-0.29293	0.667	0.4067	0.7812
0.15	2.96622	-0.02193	-1.3646	-0.0265	0.0545	-0.48313	-0.39551	0.6796	0.3893	0.7832
0.20	2.73872	-0.03462	-1.28877	0	0.0493	-0.65315	-0.44644	0.6645	0.3842	0.7676
0.30	2.3015	-0.05672	-1.17072	0	0.0469	-0.82609	-0.45730	0.6599	0.3816	0.7623
0.40	1.89372	-0.07684	-1.0653	0	0.04	-0.89517	-0.43008	0.6697	0.3962	0.7781
0.50	1.67127	-0.0949	-1.01909	0	0.0271	-0.94614	-0.37408	0.6512	0.4021	0.7653
0.75	0.95211	-0.12347	-0.88393	0	0.0141	-1.00786	-0.28957	0.6744	0.4043	0.7863
1.00	0.52349	-0.14345	-0.81838	0	0	-1.01331	-0.28702	0.6787	0.3943	0.7849
1.50	-0.01867	-0.17187	-0.75751	0	0	-0.98071	-0.24695	0.7164	0.3799	0.8109
2.00	-0.42891	-0.19029	-0.72033	0	-0.009	-0.91007	-0.17336	0.7254	0.3717	0.8151
3.00	-1.05642	-0.21392	-0.69085	0	-0.0683	-0.85793	-0.13336	0.6997	0.4046	0.8083
4.00	-1.37536	-0.23848	-0.66482	0	-0.2231	-0.75645	-0.07749	0.6196	0.3566	0.7149
PGV	5.61201	-0.0998	-0.98388	-0.0616	0.063	-0.72057	-0.19688	0.6014	0.3311	0.6865

Table 4 continued

Period(s)	a ₁	a ₃	a ₄	a ₈	a ₉	b ₁	b ₂	ϕ	τ	σ
(b)										
PGA	2.52977	-0.05496	-1.31001	-0.1091	0.0937	-0.41997	-0.28846	0.6375	0.3581	0.7312
0.01	2.54832	-0.05434	-1.31268	-0.1115	0.0953	-0.41729	-0.28685	0.6389	0.3607	0.7337
0.02	2.6442	-0.05452	-1.33135	-0.104	0.1029	-0.39998	-0.28241	0.6434	0.3615	0.738
0.03	2.77723	-0.05196	-1.35509	-0.0973	0.1148	-0.34799	-0.26842	0.6569	0.3617	0.7499
0.04	2.92666	-0.04657	-1.38259	-0.0884	0.1073	-0.27572	-0.24759	0.6693	0.353	0.7567
0.05	3.09355	-0.04168	-1.41008	-0.0853	0.1052	-0.21231	-0.22385	0.6773	0.3612	0.7676
0.075	3.38462	-0.03506	-1.44268	-0.0779	0.0837	-0.14427	-0.17525	0.6791	0.3853	0.7808
0.10	3.61906	-0.03936	-1.4687	-0.0749	0.0761	-0.27064	-0.29293	0.6851	0.416	0.8015
0.15	3.70477	-0.05156	-1.44613	-0.0265	0.0545	-0.48313	-0.39551	0.7011	0.3978	0.8061
0.20	3.40112	-0.0621	-1.3577	0	0.0493	-0.65315	-0.44644	0.6922	0.3965	0.7977
0.30	2.87449	-0.08126	-1.22665	0	0.0469	-0.82609	-0.45730	0.6897	0.3894	0.792
0.40	2.40119	-0.09885	-1.11318	0	0.04	-0.89517	-0.43008	0.6971	0.4012	0.8043
0.50	2.16953	-0.11604	-1.06795	0	0.0271	-0.94614	-0.37408	0.6751	0.4065	0.788
0.75	1.38296	-0.14169	-0.92585	0	0.0141	-1.00786	-0.28957	0.6937	0.4011	0.8013
1.00	0.94162	-0.16069	-0.86109	0	0	-1.01331	-0.28702	0.6922	0.3965	0.7977
1.50	0.36315	-0.1879	-0.79498	0	0	-0.98071	-0.24695	0.7287	0.3821	0.8228
2.00	-0.02806	-0.20666	-0.7626	0	-0.009	-0.91007	-0.17336	0.7333	0.3734	0.8229
3.00	-0.64241	-0.23038	-0.73634	0	-0.0683	-0.85793	-0.13336	0.7051	0.4115	0.8164
4.00	-0.93329	-0.25756	-0.7121	0	-0.2231	-0.75645	-0.07749	0.6241	0.3659	0.7235
PGV	6.13498	-0.12091	-1.04013	-0.0616	0.063	-0.72057	-0.19688	0.6143	0.3485	0.7063

Table 4 continued

Period(s)	a ₁	a ₃	a ₄	a ₈	a ₉	b ₁	b ₂	ϕ	τ	σ
(c)										
PGA	3.26685	-0.04846	-1.47905	-0.1091	0.0937	-0.41997	-0.28846	0.6475	0.3472	0.7347
0.01	3.28656	-0.04784	-1.48197	-0.1115	0.0953	-0.41729	-0.28685	0.6492	0.3481	0.7366
0.02	3.38936	-0.04796	-1.50214	-0.104	0.1029	-0.39998	-0.28241	0.6543	0.3508	0.7424
0.03	3.53155	-0.04537	-1.52781	-0.0973	0.1148	-0.34799	-0.26842	0.6685	0.3526	0.7558
0.04	3.68895	-0.03991	-1.55693	-0.0884	0.1073	-0.27572	-0.24759	0.6816	0.3513	0.7668
0.05	3.86581	-0.0349	-1.58672	-0.0853	0.1052	-0.21231	-0.22385	0.6899	0.3659	0.7809
0.075	4.18224	-0.02826	-1.62527	-0.0779	0.0837	-0.14427	-0.17525	0.6881	0.3942	0.793
0.10	4.4375	-0.03256	-1.65601	-0.0749	0.0761	-0.27064	-0.29293	0.6936	0.4122	0.8068
0.15	4.52949	-0.04509	-1.63467	-0.0265	0.0545	-0.48313	-0.39551	0.7048	0.3779	0.7997
0.20	4.1775	-0.05565	-1.53574	0	0.0493	-0.65315	-0.44644	0.6954	0.3848	0.7948
0.30	3.57698	-0.0749	-1.38832	0	0.0469	-0.82609	-0.45730	0.6934	0.3896	0.7954
0.40	3.03752	-0.09243	-1.26045	0	0.04	-0.89517	-0.43008	0.7037	0.3894	0.8043
0.50	2.77997	-0.10964	-1.20953	0	0.0271	-0.94614	-0.37408	0.6821	0.4017	0.7916
0.75	1.91625	-0.13547	-1.05027	0	0.0141	-1.00786	-0.28957	0.7028	0.389	0.8033
1.00	1.43982	-0.15427	-0.97812	0	0	-1.01331	-0.28702	0.7022	0.3826	0.7997
1.50	0.83007	-0.18248	-0.90319	0	0	-0.98071	-0.24695	0.7378	0.3758	0.828
2.00	0.40614	-0.20136	-0.86343	0	-0.009	-0.91007	-0.17336	0.7446	0.3676	0.8304
3.00	-0.22534	-0.22564	-0.83314	0	-0.0683	-0.85793	-0.13336	0.7154	0.4019	0.8206
4.00	-0.51893	-0.25256	-0.80922	0	-0.2231	-0.75645	-0.07749	0.6364	0.3318	0.7177
PGV	6.72743	-0.11474	-1.17694	-0.0616	0.063	-0.72057	-0.19688	0.628	0.3312	0.71

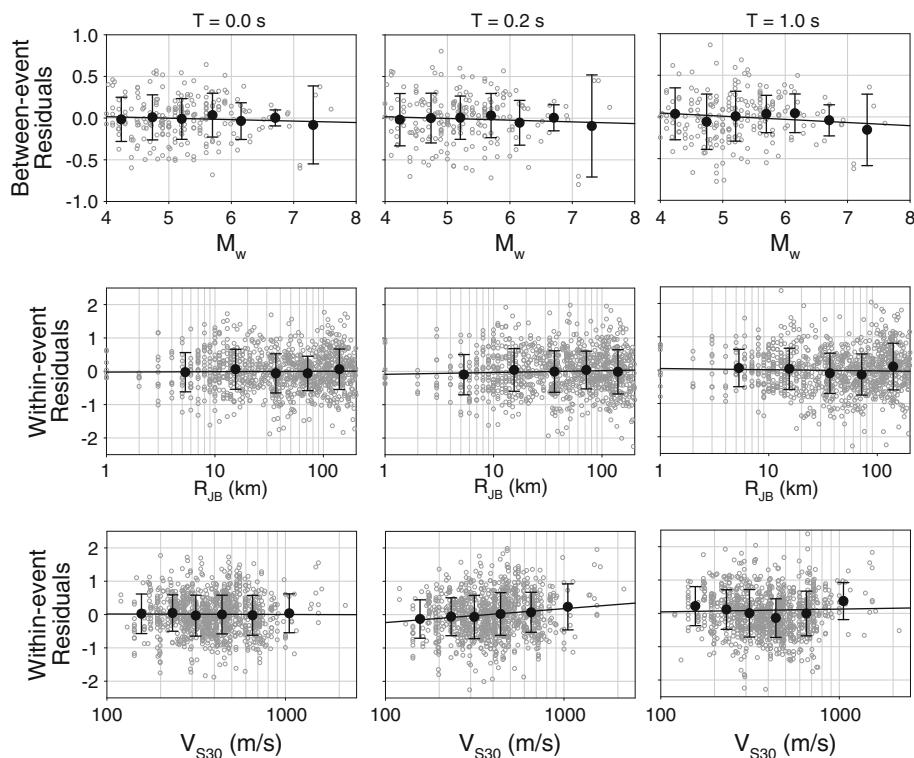
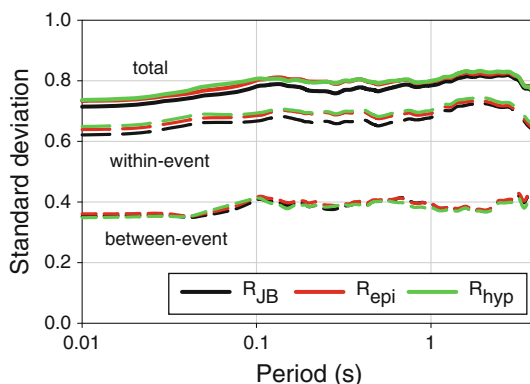


Fig. 5 Residual plots for R_{JB} model.

Fig. 6 Components of the standard deviation of the models.



obtained are almost independent of period and the total sigmas are similar to those of the NGA models and those of the previous pan-European model by [Akkar and Bommer \(2010\)](#).

As with the study of [Bommer and Akkar \(2012\)](#), it is perhaps surprising that the sigma values for the point-source based models are not larger compared to that for the extended-source based model. The reason probably lies in the relative lack of data from earthquakes of $M_w > 6$ recorded at short distances (less than 10–15 km). An estimate of the true variability in the R_{epi} model could be obtained by generating ground-motion fields at dense grid

points around various hypothetical ruptures (with dimensions appropriate to the earthquake magnitude), predicting the motions (at various exceedance levels) using the R_{JB} model. The epicentral distances could then be calculated (making appropriate assumptions about the distribution of unilateral and bilateral ruptures) and regressions performed in R_{epi} to obtain sigma values that may better reflect the added variability from using point-source distance metrics. The sigma model developed in this way may need to be magnitude- and/or distance-dependent, and the values would then likely differ from those presented herein only for larger magnitudes and relatively short epicentral distances.

5 Predictions and comparison with other models

Figure 7 compares the magnitude-scaling of the proposed model with the magnitude scaling of Akkar and Bommer (2010), which used data from M_w 5 upwards, and Bommer et al. (2007), which used data from M_w 3 upwards. The comparisons are made for a generic rock site ($V_{S30} = 750$ m/s) located $R_{JB} = 10$ km from a strike-slip fault. We considered PGA (PSA at $T = 0$ s) as well as PSA at $T = 0.2$ s and $T = 1$ s in comparisons as they are widely used spectral ordinates to construct smoothed spectrum in several seismic design codes. Only the proposed model and Akkar and Bommer (2010) are compared for PSA at $T = 1$ s as the Bommer et al. (2007) GMPE predicts spectral ordinates up to 0.5 s. The proposed model and Bommer et al. (2007) follow very similar trends for $M_w \geq 5$ although the lower magnitude limit of our strong-motion database is one magnitude unit above that used for the derivation of the Bommer et al. (2007) model. Our new model appears to overestimate the spectral ordinates for $M_w < 5$ if compared to Bommer et al. (2007), possibly due to the differences in the lower magnitude bounds of these models. This interpretation would suggest that the phenomenon of empirical models over-estimating ground-motion amplitudes at the lower magnitude limit of the dataset persists to smaller magnitudes. However, this is almost entirely predicated on the comparison with Bommer et al. (2007), which may give excessive credence to that earlier model. It may equally be the case that by extending the lower magnitude limit of the database to M_w 4, we have better constrained the (more) linear part of the magnitude scaling and therefore the new model may perform satisfactorily at this lower limit. The Akkar and Bommer (2010) GMPE overestimates the ground-motion amplitudes in the magnitude range of $4 \leq M_w \leq 6.5$ with respect to the other two models. This model constitutes the lower bound of the three sets of predictions at higher magnitude levels (i.e., $M_w > 6.5$). Similar to above explanations, the higher ground-motion estimations of Akkar and Bommer (2010) are directly related to the lower magnitude limit of this model (i.e., $M_w > 5$). The quadratic-magnitude functional form of the Akkar and Bommer (2010) model predicts over-saturation at large magnitudes, which was a characteristic of the database used at the time (similar patterns were observed in the early versions of the NGA equations, which the model developers addressed by forcing the models not to pass into over-saturation).

Figure 8 compares the spectral amplitude ratios of our ground-motion models as well as those of previously published GMPEs for different styles-of-faulting. The GMPEs used for comparison are Akkar and Bommer (2010)–AB10, with its extension for $T < 0.05$ s (Bommer et al. 2012)–BAD12, as well as four NGA models: Abrahamson and Silva (2008)–AS08, Boore and Atkinson (2008)–BA08, Campbell and Bozorgnia (2008)–CB08, and Chiou and Youngs (2008)–CY08. The fault rupture is assumed to reach the surface ($Z_{TOR} = 0$ km) while computing the spectral amplitude ratios of AS08, CB08 and CY08. As one can infer from these plots, the normal-to-strike-slip spectral amplitude ratios (N:SS) of our models yield a pattern that is fairly consistent with the predictions of AS08, CB08 and AB10. This is not the

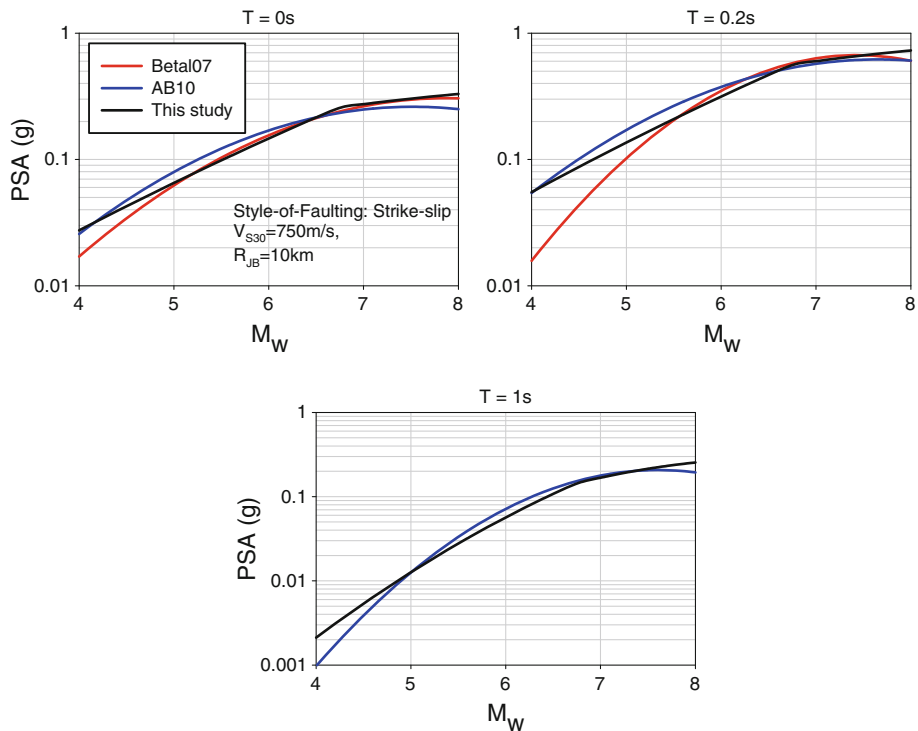


Fig. 7 Magnitude-scaling comparisons between two previous pan-European GMPEs (Bommer et al. 2007–Betal07 and Akkar and Bommer 2010–AB10) and the proposed model. Comparisons are made for a rock site ($V_{S30} = 750$ m/s) located $R_{JB} = 10$ km from a strike-slip fault.

case for the N:SS ratios predicted by BA08 and CY08 as they show large differences in terms of N:SS ratios with the GMPEs presented in this study and the other NGA models. Moreover, the N:SS ratios predicted by BA08 and CY08 diverge from each other and follow completely different trends after $T = 0.75$ s. The reverse-to-strike-slip (R:SS) ratio estimations of the considered GMPEs show significant discrepancies over the period range given in Fig. 8. Although the reverse-to-strike-slip spectral (R:SS) ratios of AS08 and BA08 are similar for $T \leq 1$ s, they diverge from each towards longer periods. The proposed model and the former pan-European GMPE, AB10, only show similar R:SS ratios for $1.5 \text{ s} \leq T \leq 3 \text{ s}$. The period-dependent R:SS estimations of CB08 and CY08 have similar shapes but their amplitudes differ significantly from each other.

The observed model differences in the spectral amplitude ratio predictions of different styles-of-faulting warrant some discussion here. Several factors may be contributing to these observations, and we do not believe that we can currently identify the definitive reason(s) behind these observations but rather offer a number of remarks for consideration by the reader. Although most previous equations have predicted larger motions from strike-slip than from normal earthquakes, the differences have generally been small. Westaway and Smith (1989) concluded that there were no systematic differences between the two styles-of-faulting, and Spudich et al. (1999) reached the same conclusion for earthquakes in extensional regimes, although they noted that these were systematically lower than motions from compressional regions. Therefore, style-of-faulting effects may represent or be concealed by regional differ-

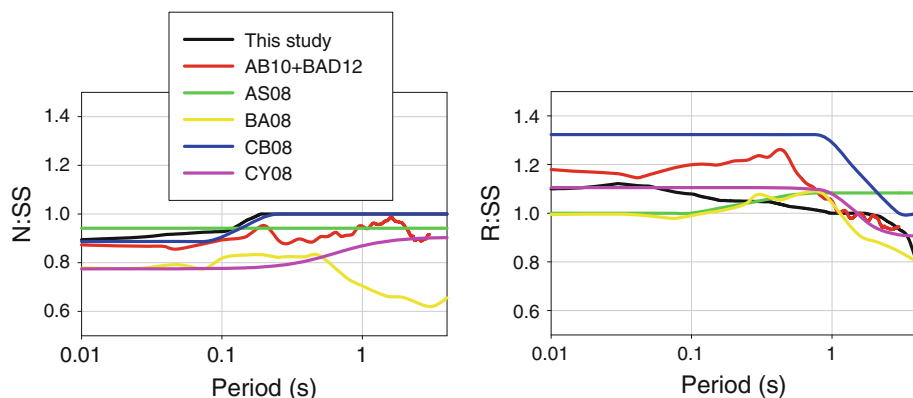
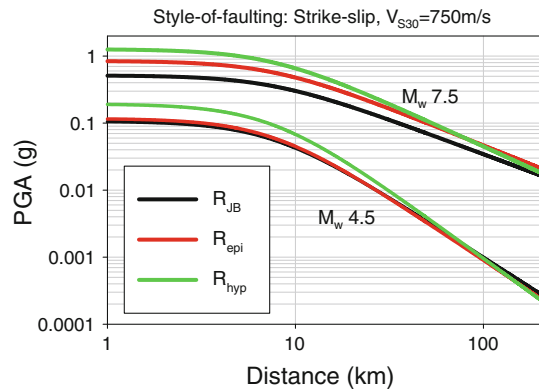


Fig. 8 Period dependent normal-to-strike-slip (*left panel*) and reverse-to-strike-slip (*right panel*) spectral ordinate ratios of different GMPEs.

ences in ground motions. Similarly, the style-of-faulting effect can trade-off with effects such as the fact that buried ruptures tend to produce higher amplitudes of motion than ruptures that break the surface (Kagawa et al. 2004), reflected in the NGA models by the inclusion of a parameter reflecting the depth-to-the-top-of-rupture (Z_{TOR}). This trade-off is related to the fact that deeper events are likely to be associated with higher stress drop, which may have a more pronounced effect than the increased separation of source and site. Another factor that must be considered is the limitations of strong-motion databases in terms of different rupture mechanisms. For example, normal-faulting earthquakes are poorly represented in the datasets used for the NGA models, which is not the case for this pan-European database. On the other hand, in our current database, nearly all records from events with $M_w > 7$ are from strike-slip earthquakes with none from normal events and only two from reverse events. Thus, it may also be the case that such non-uniform distribution of rupture mechanisms in the databases contributes to the observed discrepancies in style-of-faulting ratios. The variation in style-of-faulting ratios under the influence of strong-motion database features is discussed in Sandikkaya and Akkar (2012) by using alternative subsets of the strong-motion database used in this study.

Figure 9 shows the distance scaling of the proposed GMPEs for two magnitude levels (M_w 4.5 and M_w 7.5) at $T = 0$ s (PGA). The reference site condition ($V_{S30} = 750$ m/s) and strike-slip rupture mechanism are considered in the comparative plots. As expected the models using R_{epi} and R_{JB} overlap each other for M_w 4.5 as R_{epi} and R_{JB} are practically the same when the seismic energy radiation is concentrated at a relatively small rupture area (point-source). The discrepancy between the R_{epi} and R_{JB} models increases for the M_w 7.5 scenario as the rupture dimensions lead to very large differences between average values of the R_{epi} and R_{JB} distance metrics. At short distances from the source the R_{epi} model results in higher predicted ground motions because R_{JB} would be equal to or less than R_{epi} , thus reducing the ground-motion amplitudes for a given distance. As the source-to-site distance increases the rupture size losses its significance even for large magnitudes, thus the difference between R_{epi} and R_{JB} diminishes and the predicted ground motions become almost equal for these models. On such a plot, where each GMPE is plotted against its own distance metric, the proposed GMPE using R_{hyp} predicts apparently larger ground motions regardless of magnitude for distances closer to the site because at comparable horizontal distances, the other models are implicitly accounting for the attenuation over the focal depth.

Fig. 9 Distance scaling of the proposed ground-motion models.



As the source-to-site distance increases the difference between R_{hyp} and the other distance measures becomes insignificant.

The distance scaling of the predictive model using R_{JB} is presented in more detail in Fig. 10. The plots on this figure show the median estimations of PGA and spectral ordinates at $T = 0.2$ s, $T = 1$ s and $T = 4$ s for $M_w > 6$. As in all other comparative plots, the distance-dependent median estimations are for a rock site of $V_{S30} = 750$ m/s and strike-slip fault. The plots do not show decreasing amplitudes at very short distances. For magnitudes $M_w 7.5$ and above, the short- and intermediate-period spectral ordinates (i.e., PGA, PSA at $T = 0.2$ and 1 s) tend to converge and overlap each other. This phenomenon is the so-called magnitude saturation but our model gives no indication of magnitude oversaturation that results in a decreasing trend in spectral ordinates at large magnitudes and short distances. Predictive models that use a reference distance term in their distance scaling function can impose magnitude oversaturation in ground-motion estimations (Dr. David M. Boore, *personal communication*, 2013). Thus, our functional form is not tailored for capturing magnitude oversaturation effects.

When presenting new GMPEs it is common to compare predictions in terms of median spectra to those from previous well-known GMPEs. The median estimations of the R_{JB} model are compared with the NGA GMPEs and the previous pan-European GMPE of Akkar and Bommer (2010) with its extension for $T < 0.05$ s (Bommer et al. 2012) in Fig. 11. Two magnitude levels ($M_w 5$ and $M_w 7$) are chosen in the comparisons that can encompass small-to-large size events in Europe and surrounding regions. The site is assumed to be located $R_{JB} = 30$ km from a 90° dipping strike-slip fault and all common Eurocode 8 site classes (A as $V_{S30} = 800$ m/s, B as $V_{S30} = 525$ m/s, C as $V_{S30} = 255$ m/s and D as $V_{S30} = 180$ m/s) are taken into account to observe the behavior of R_{JB} model together with the other GMPEs. For the rupture geometry of the chosen scenario, R_{JB} and R_{rup} are equivalent hence no adjustments are needed to compare predictions from the NGA models. Surface rupture is assumed and other estimator parameters used by NGA models are estimated from Kaklamanos et al. (2011). The plots indicate that the median estimations of the R_{JB} model are comparable with the other GMPEs for all magnitude and site classes considered in the case study. Our model tends to estimate relatively small spectral amplitudes, particularly at short periods, for small magnitudes ($M_w 5$).

As a variant on the previous figure, Fig. 12 compares predicted spectra from all three proposed models to those estimated by the GMPEs in Fig. 11 as well as those that use either R_{epi} or R_{hyp} . The selected earthquake scenarios generically represent the moderate seismicity

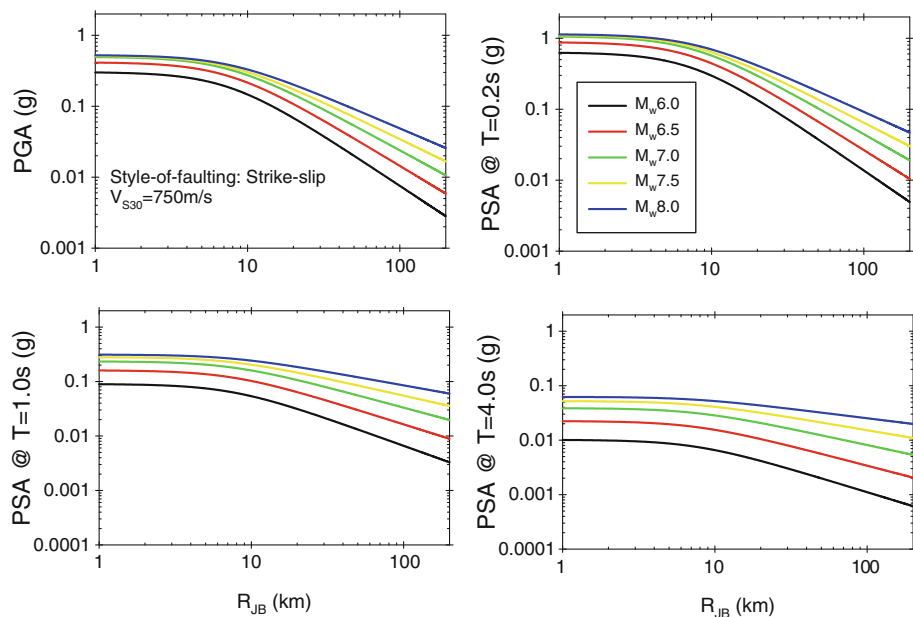


Fig. 10 Distance scaling of R_{JB} model at different spectral ordinates (PGA, PSA at $T = 0.2, 1.0$ and 4.0 s) for magnitudes above 6.

(median + 0.5σ for an M_w 6 event) and high seismicity (median + 1σ for an M_w 7 event) regions in Europe and are used in the comparisons to give a more complete picture of the influence of adopting these new R_{JB} , R_{epi} and R_{hyp} models over those already in the literature. The spectra predicted by these new models are generally comparable to those from previous GMPEs but are often higher (particularly for M_w 6 and at short periods).

As a test of our model outside the ‘comfort zone’ (Akkar and Bommer 2010) Fig. 13 presents predicted 84th percentile spectra for M_w 8 at $R_{JB} = 5$ km and $R_{JB} = 200$ km for a rock site ($V_{S30} = 800$ m/s). The predicted spectra are compared with the global GMPEs considered in this study. The comparisons for $R_{JB} = 5$ km indicate good agreement between the proposed model and the other GMPEs although our spectral ordinates are slightly higher in the short-period range. The trend in the predicted spectrum at $R_{JB} = 200$ km is roughly similar to the compared NGA models. However, the NGA models also show great variations with respect to one another at this distance, which may suggest that the data on which they are based, and the way the models are derived, means that the decay at such distances has not been well constrained in all cases. Our model is generally on the high side for M_w 8, and envelopes the other spectra at longer periods, probably due to its larger SDs with respect to the other compared GMPEs. Most of the NGA GMPEs (except for BA08) impose smaller sigma at large magnitudes due to their magnitude-dependent SD modeling.

6 Discussion and conclusions

In this paper we have presented new empirical GMPEs for the prediction of PGA, PGV and ordinates of horizontal spectral acceleration at oscillator periods from 0.01 to 4 s derived from strong-motion recordings obtained in the Mediterranean region and the Middle East.

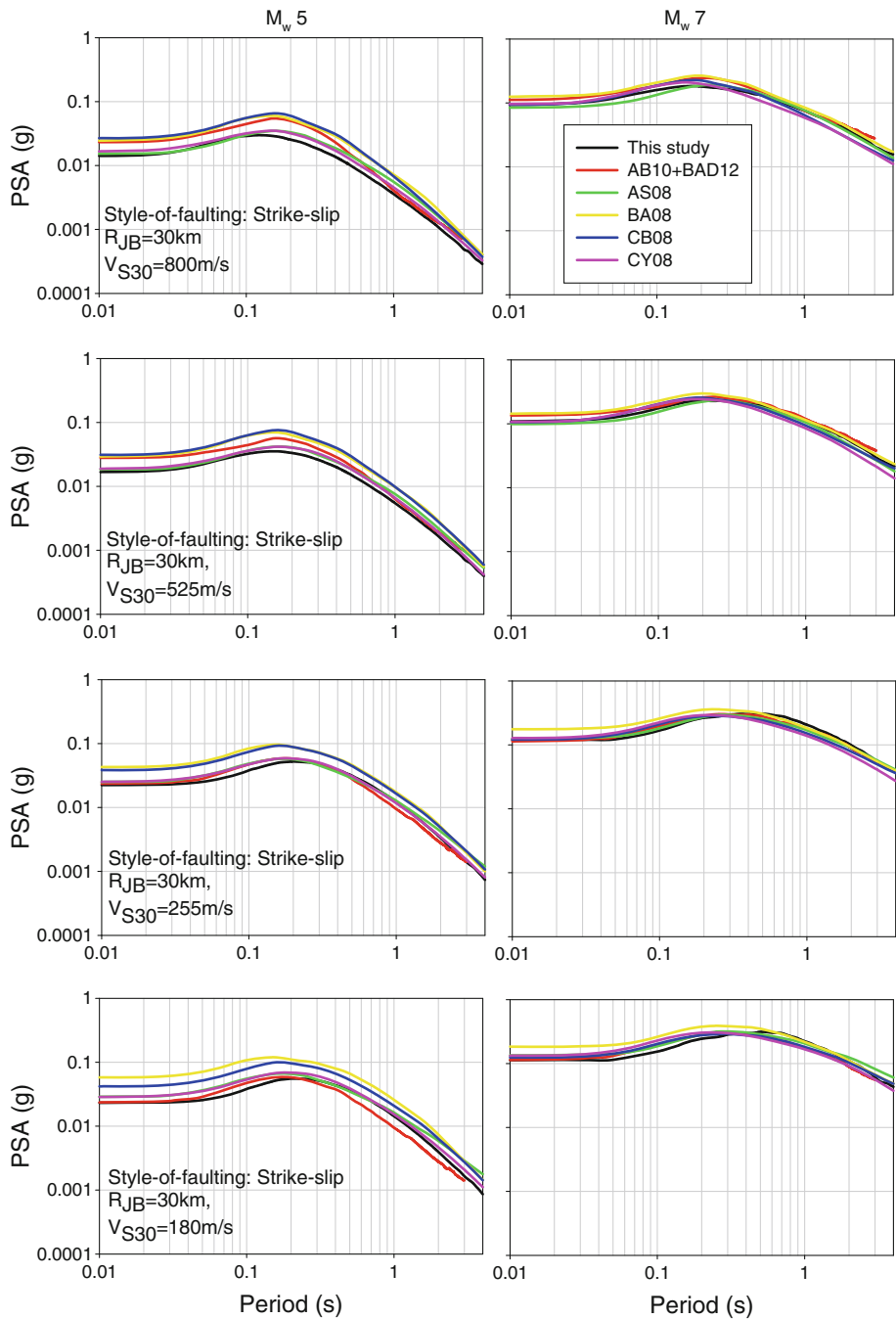


Fig. 11 Median estimation comparisons of R_{JB} model with other GMPEs.

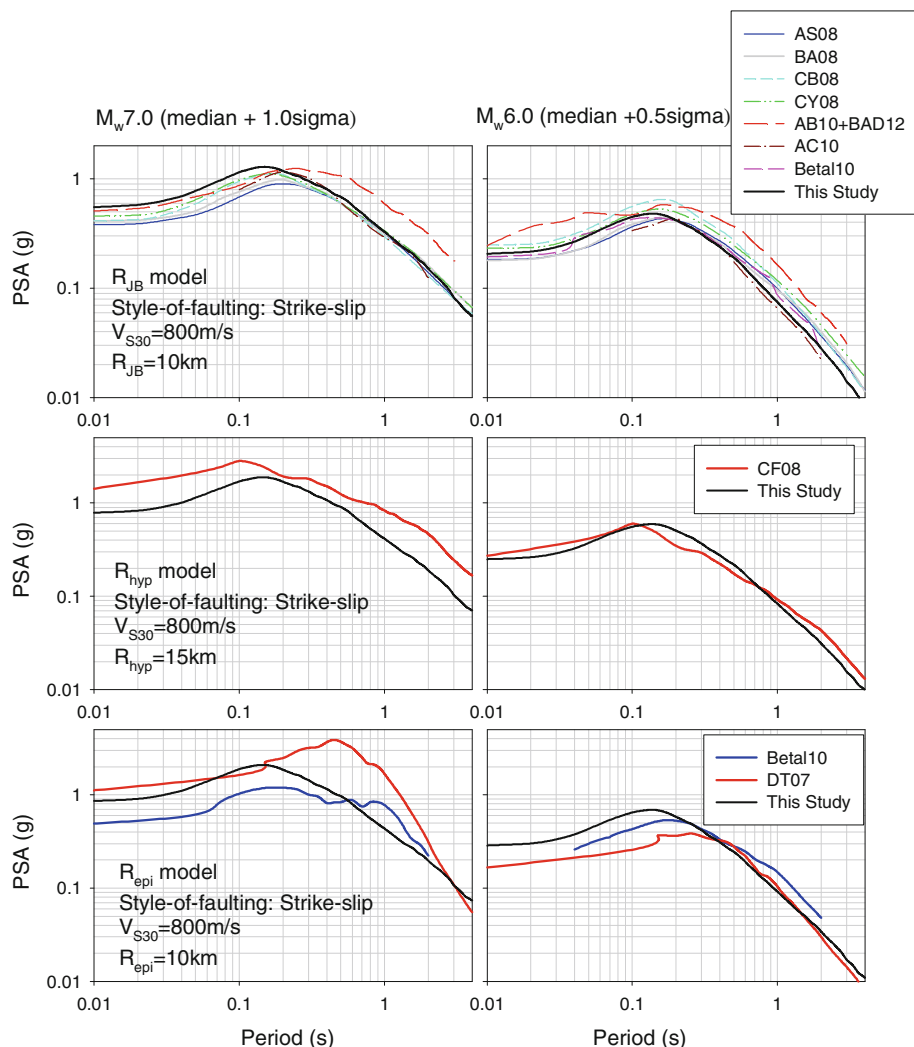


Fig. 12 Comparison of predicted spectra from the new models and some global, regional and local models. This comparison is for a surface-rupturing vertically-dipping strike-slip fault with a focal depth of 11 km and an epicenter at the center of the surface trace ($R_{JB} = R_{epi} = R_{rup} = 10$ km and $R_{hyp} = 15$ km). The site is a generic rock site with $V_{S30} = 800$ m/s. The abbreviations AC10, Betal10, CF08 and DT07 stand for Akkar and Çağnan (2010), Bindi et al. (2010), Cauzzi and Faccioli (2008) and Danciu and Tselentis (2007) GMPEs, respectively.

We believe the models can be applied to earthquakes (of focal depth not greater than 30 km) with moment magnitudes in the range from 4 to 8, although we acknowledge that there is a possibility of over-estimating motions at the lower limit, and there is some uncertainty at the upper end, which is poorly constrained by the data (which only extends to M_w 7.6). The models include the influence of the style-of-faulting and are well constrained for normal, strike-slip and reverse ruptures. To facilitate hazard analyses using both fault and area sources, three models are presented using the R_{epi} , R_{hyp} and R_{JB} distance metrics; the models are

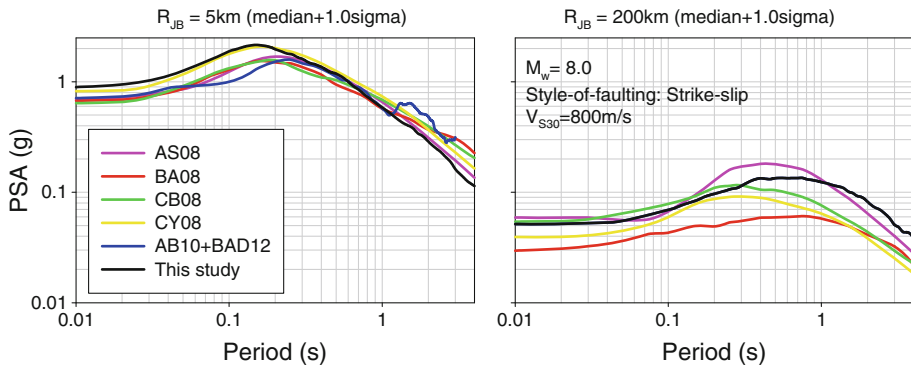


Fig. 13 Comparisons of proposed model with global GMPEs for an earthquake of M_w 8.0 showing 84-percentile values on rock site ($V_{S30} = 800\text{ m/s}$) at 5 km (left) and 200 km (right).

applicable up to at least 200 km, and may be extrapolated beyond this limit with some caution. The models include nonlinear site response effects and can be applied for sites with V_{S30} values from 150 to 1,200 m/s.

A topic of considerable debate in the recent literature is the nature of the sigma model to be used with GMPEs (Strasser et al. 2009; Al Atik et al. 2010). One pressing question is whether aleatory variability of ground motions from small earthquakes is inherently larger than that of ground motions from large events. For the development of this model we chose to assume a homoscedastic (magnitude-independent) sigma even though residual plots suggested that sigma could be lower for larger events. This decision was made since we do not feel that there are sufficient data from large earthquakes to obtain a robust estimate of the coefficients of a more sophisticated sigma model. In addition, although much effort has been made in improving the metadata of our strong-motion database we feel that some of the apparent scatter in the residual plots for small earthquakes is coming from uncertainties in the independent parameters (e.g., Figure 4.13 of Moss 2009). There are, however, possible mechanisms for magnitude-dependent sigma. Figures 2 and 3 of Douglas and Jousset (2011) suggest that variations in kappa, κ , (Anderson and Hough 1984) between sites could be partly responsible for short-period ground-motion variability increasing with decreasing magnitude.

Although these new GMPEs are relatively complex compared to previous generations of pan-European ground-motion models, they are still simple representations of very complex processes. The source characteristics of earthquakes are represented only by magnitude and style-of-faulting, and the predictions may well be biased if the dataset from which the equations have been derived has not sampled, for example, the full range of stress drops from earthquakes of a given magnitude and rupture mechanism in the region. Such considerations lead to recognition of epistemic uncertainty in the median ground-motion predictions, which necessitates the combination of several GMPEs within a logic-tree framework (Bommer et al. 2005). The question that then immediately arises is: which other models should be combined with these GMPEs for PSHA in Europe and the Middle East?

These new equations supersede previous GMPEs derived for Europe and the Middle East, and address shortcomings identified in those models. Moreover, the formulation of the new equations covering broader ranges of response period, earthquake magnitude and distance, means that the former equations are not compatible with the new models. For PSHA studies in Europe and the Middle East, one option would be to construct logic-trees

by combining these new GMPEs with the Next Generation of Attenuation (NGA) models of [Abrahamson and Silva \(2008\)](#); [Boore and Atkinson \(2008\)](#); [Campbell and Bozorgnia \(2008\)](#), and [Chiou and Youngs \(2008\)](#). These NGA models are broadly consistent with the new model in terms of parameterization, and it has been demonstrated that the NGA models are broadly applicable in Europe ([Stafford et al. 2008](#)), although [Scasserra et al. \(2009\)](#) and [Akkar and Çağnan \(2010\)](#) found some systematic differences between the NGA predictions and strong-motion data from Italy and Turkey, respectively. In addition to recommending the use of the NGA models, [Bommer et al. \(2010\)](#) identified the GMPEs of [Zhao et al. \(2006\)](#), derived predominantly from Japanese data, as another candidate for selection within PSHA for shallow crustal seismicity. Additional logic-tree branches could be populated using local GMPEs, provided these were compatible in terms of parameter definitions. An alternative approach would be to use the new GMPEs as ‘backbones’ and create additional logic-tree branches by scaling the median predictions up and down as appropriate to reflect possible differences in median stress drops, etc.. The scaling factors could also be distance-dependent if potential differences in attenuation needed to be captured as well. Such approaches are being used more and more widely in PSHA studies and this is likely to become standard practice over the coming years ([Bommer 2012](#)). The construction of a logic-tree for ground-motion predictions by scaling a single backbone GMPE offers several advantages, including obviating the need for any adjustments for parameter compatibility among the equations and a more transparent relationship between branch weights and the resulting distributions of median ground-motion amplitudes. Another advantage, particular relevant to PSHA for safety-critical facilities, is that it allows a wider range of epistemic uncertainty to be captured than that represented by simply assembling available models for a region.

The database from which these new models have been derived is dominated by recordings from Italy, Turkey and Greece, but we believe that the equations can be used with confidence for crustal earthquakes in seismically active areas of southern Europe and the Middle East. A question that arises, however, is whether these models will have applicability to more stable regions, such as northwest Europe? Although NW Europe may be considered to be a stable region, this has not always led those conducting seismic hazard analyses to adopt GMPEs from other stable continental regions such as Central and Eastern United States: for example, in developing hazard maps for the UK, [Musson and Sargreant \(2007\)](#) adopted one NGA equation and one of the predecessors of the model presented in this paper. Whether or not the new models may be applicable to any particular region could be explored using any available local recordings and any one of the available methods for ranking GMPE performance ([Scherbaum et al. 2004, 2009](#); [Kale and Akkar 2013](#)), although if only recordings from small-magnitude earthquakes are available locally, the results of such procedures must be interpreted with caution. Consideration should always be given to the application of the hybrid-empirical approach of [Campbell \(2003\)](#) to render the selected equations more applicable to the target region, as done, for example, by [Douglas et al. \(2006\)](#) for southern Norway and southern Spain. The key issue that must be borne in mind is that epistemic uncertainty in ground-motion prediction in such regions must, inevitably, be higher than in more active areas with more abundant data and this should be reflected in the logic-trees developed for PSHA, whether using the ‘backbone’ approach discussed above and/or by combining adjusted empirical models with local stochastic equations, such as [Rietbrock et al. \(2013\)](#) for the case of the UK, for example. The models presented here could be the last generation of pan-European GMPEs before the development of truly global ground-motion models for shallow crustal seismicity. This would require the development of a global database in the style of the NGA database ([Chiou et al. 2008](#)) with consistent and reliable metadata for records from all regions.

To help in the correct implementation of our models, tables of coefficients and SDs are available as Electronic Supplements to this paper. In addition, we provide Excel and Matlab subroutines to evaluate our models. Finally, tables of predicted median values and their associated SDs for various earthquake scenarios are available on request to check evaluations of the models within quality assurance procedures (e.g., for nuclear power projects).

Acknowledgments The work presented in this article has been mainly developed within the SHARE (Seismic Hazard Harmonization in Europe) Project funded under contract 226967 of the EC-Research Framework Programme FP7, and within the Seismic Ground Motion Assessment (SIGMA) project. We benefitted significantly from the suggestions and comments of Dr. John Douglas, Professor Frank Scherbaum and Professor Fabrice Cotton during early discussions regarding these new models, particularly within the context of the SHARE Project. We are very grateful to David M. Boore and an anonymous reviewer for constructive feedback on the original version of this paper that assisted us in improving the final presentation of the new models.

References

- Abrahamson NA, Silva W (2008) Summary of the Abrahamson and Silva NGA ground-motion relations. *Earthq Spectra* 24:67–97
- Abrahamson NA, Youngs RR (1992) A stable algorithm for regression analyses using the random effects model. *Bull Seismol Soc Am* 82:505–510
- Akkar S, Bommer JJ (2006) Influence of long-period filter cut-off on elastic spectral displacements. *Earthq Eng Struct Dyn* 35:1145–1165
- Akkar S, Bommer JJ (2007a) Prediction of elastic displacement response spectra at multiple damping levels in Europe and the Middle East. *Earthq Eng Struct Dyn* 36:1275–1301
- Akkar S, Bommer JJ (2007b) Empirical prediction equations for peak ground velocity derived from strong-motions records from Europe and the Middle East. *Bull Seismol Soc Am* 97:511–530
- Akkar S, Bommer JJ (2010) Empirical equations for the prediction of PGA, PGV and spectral accelerations in Europe, the Mediterranean and the Middle East. *Seismol Res Lett* 81:195–206
- Akkar S, Çağnan Z (2010) A local ground-motion predictive model for Turkey, and its comparison with other regional and global ground-motion. *Bull Seismol Soc Am* 100:2978–2995
- Akkar S, Kale Ö, Yenier E, Bommer JJ (2011) The high-frequency limit of usable response spectral ordinates from filtered analogue and digital strong-motion accelerograms. *Earthq Eng Struct Dyn* 40:1387–1401
- Akkar S, Sandikkaya MA, Şenyurt M, Azari SA, Ay BÖ (2013) Reference database for seismic ground-motion in Europe (RESORCE). *Bull Earthq Eng* (submitted to this issue)
- Al Atik L, Abrahamson NA, Bommer JJ, Scherbaum F, Cotton F, Kuehn N (2010) The variability of ground-motion prediction models and its components. *Seismol Res Lett* 81:783–793
- Ambraseys NN, Douglas J, Sarma SK, Smit PM (2005) Equations for the estimation of strong ground motion from shallow crustal earthquakes using data from Europe and the Middle East: horizontal peak ground acceleration and spectral acceleration. *Bull Earthq Eng* 3:1–53
- Ambraseys NN, Simpson KA, Bommer JJ (1996) The prediction of horizontal response spectra in Europe. *Earthq Eng Struct Dyn* 25:371–400
- Anderson JG, Hough SE (1984) A model for the shape of the Fourier amplitude spectrum of acceleration at high frequencies. *Bull Seismol Soc Am* 74:1969–1993
- Atkinson GM, Morrison M (2009) Observations on regional variability in ground-motion amplitude for small-to-moderate magnitude earthquakes in North America. *Bull Seismol Soc Am* 99:2393–2409
- Berge-Thierry C, Cotton C, Scotti O, Griot-Pommeret D-A, Fukushima Y (2003) New empirical attenuation laws for moderate European earthquakes. *J Earthq Eng* 7:193–222
- Bindi D, Luzi L, Massa M, Pacor F (2010) Horizontal and vertical ground motion prediction equations derived from the Italian Accelerometric Archive (ITACA). *Bull Earthq Eng* 8:1209–1230
- Bommer JJ (2012) The challenge of building logic trees for probabilistic seismic hazard analysis. *Earthq Spectra* 28:1723–1735
- Bommer JJ, Akkar S (2012) Consistent source-to-site distance metrics in ground-motion prediction equations and seismic source models for PSHA. *Earthq Spectra* 28:1–15
- Bommer JJ, Akkar S, Kale Ö (2011) A model for vertical-to-horizontal response spectral ratios for Europe and the Middle East. *Bull Seismol Soc Am* 101:1783–1806
- Bommer JJ, Akkar S, Drouet S (2012) Extending ground-motion prediction equations for spectral ordinates to higher response frequencies. *Bull Earthq Eng* 10:379–399

- Bommer JJ, Alarcón JE (2006) The prediction and use of peak ground velocity. *J Earthq Eng* 10:1–31
- Bommer JJ, Douglas J, Scherbaum F, Cotton F, Bungum H, Fäh D (2010b) On the selection of ground-motion prediction equations for seismic hazard analysis. *Seismol Res Lett* 81:783–793
- Bommer JJ, Douglas J, Strasser FO (2003) Style-of-faulting in ground motion prediction equations. *Bull Earthq Eng* 1:171–203
- Bommer JJ, Scherbaum F (2008) The use and misuse of logic-trees in PSHA. *Earthq Spectra* 24:997–1009
- Bommer JJ, Scherbaum F, Bungum H, Cotton F, Sabetta F, Abrahamson NA (2005) On the use of logic trees for ground-motion prediction equations in seismic hazard assessment. *Bull Seismol Soc Am* 95:377–389
- Bommer JJ, Stafford PJ, Akkar S (2010a) Current empirical ground-motion prediction equations for Europe and their application to Eurocode 8. *Bull Earthq Eng* 8:5–26
- Bommer JJ, Stafford PJ, Alarcón JE, Akkar S (2007) The influence of magnitude range on empirical ground-motion prediction. *Bull Seismol Soc Am* 97:2152–2170
- Boore DM, Atkinson GM (2008) Ground-motion prediction equations for the average horizontal component of PGA, PGV, and 5%-damped PSA at spectral periods between 0.1s and 10.0s. *Earthq Spectra* 24:99–138
- Bozorgnia Y, Abrahamson NA, Campbell KW, Rowshandel B, Shantz T (2012) NGAWest2: a comprehensive research program to update ground motion prediction equations for shallow crustal earthquakes in active tectonic regions. In: Proceedings of 15th world conference on earthquake engineering paper number 2572, Lisbon, Portugal
- Campbell KW (2003) Prediction of strong ground motion using the hybrid empirical method and its use in the development of ground-motion (attenuation) relations in eastern North America. *Bull Seismol Soc Am* 93:1012–1033
- Campbell KW, Bozorgnia Y (2008) NGA ground motion model for the geometric mean horizontal component of PGA, PGV, PGD and 5%-damped linear elastic response spectra at periods ranging from 0.1 s to 10.0 s. *Earthq Spectra* 24:139–171
- Cauzzi C, Faccioli E (2008) Broadband (0.05 to 20 s) prediction of displacement response spectra based on worldwide digital records. *J Seismol* 12:453–475
- Comité Européen de Normalisation (CEN) (2004) Eurocode 8, design of structures for earthquake resistance—part 1: general rules, seismic actions and rules for buildings. European Standard NF EN 1998–1, Brussels
- Chiou B, Darragh R, Gregor N, Silva W (2008) NGA project strong-motion database. *Earthq Spectra* 24:23–44
- Chiou BS-J, Youngs RR (2008) An NGA model for the average horizontal component of peak ground motion and response spectra. *Earthq Spectra* 24:173–215
- Chiou B, Youngs R, Abrahamson N, Addo K (2010) Ground-motion attenuation model for small-to-moderate shallow crustal earthquakes in California and its implications on regionalization of ground-motion prediction models. *Earthq Spectra* 26:907–926
- Danciu L, Tselentis G-A (2007) Engineering ground-motion parameters attenuation relationships for Greece. *Bull Seismol Soc Am* 97:162–183
- Douglas J (2003) Earthquake ground motion estimation using strong-motion records: a review of equations for the estimation of peak ground acceleration and response spectral ordinates. *Earth Sci Rev* 61:43–140
- Douglas J (2011) Ground-motion prediction equations 1964–2010. Final report BRGM/RP-59356-FR
- Douglas J, Boore DM (2011) High-frequency filtering of strong-motion records. *Bull Earthq Eng* 9:395–409
- Douglas J, Bungum H, Scherbaum F (2006) Ground-motion prediction equations for southern Spain and southern Norway obtained using the composite model perspective. *J Earthq Eng* 10(1):37–72
- Douglas J, Halldórsson B (2010) On the use of aftershocks when deriving ground-motion prediction equations. In: Proceedings of the 9th U.S. national and 10th Canadian conference on earthquake engineering, paper no. 220
- Douglas J, Jousset P (2011) Modeling the difference in ground-motion magnitude-scaling in small and large earthquakes. *Seismol Res Lett* 82:504–508
- Fukushima Y, Berge-Thierry C, Volant P, Griot-Pommeret D-A, Cotton F (2003) Attenuation relation for West Eurasia determined with recent near-fault records from California, Japan and Turkey. *J Earthq Eng* 7:573–598
- Joyner WB, Boore DM (1981) Peak horizontal acceleration and velocity from strong-motion records including records from the 1979 Imperial Valley, California, earthquake. *Bull Seismol Soc Am* 71:2011–2038
- Kagawa T, Irikura K, Somerville PG (2004) Differences in ground motion and fault rupture process between the surface and buried rupture earthquakes. *Earth Planets Space* 56:3–14
- Kaklamanos J, Baise LG, Boore DM (2011) Estimating unknown input parameters when implementing the NGA ground-motion prediction equations in engineering practice. *Earthq Spectra* 27:1219–1235
- Kale Ö, Akkar S (2013) A new perspective for selecting and ranking ground-motion prediction equations (GMPEs): the euclidian distance-based ranking method. *Bull Seismol Soc Am* 103(2A):1069–1084
- Mai MP, Spudich P, Boatwright J (2005) Hypocenter locations in finite-source rupture models. *Bull Seismol Soc Am* 95:965–980

- Manighetti I, Campillo M, Sammis C, Mai PM, King G (2005) Evidence for self-similar, triangular slip distributions on earthquakes: implications for earthquake and fault mechanics. *J Geophys Res* 110:B05302. doi:[10.1029/2004JB003174](https://doi.org/10.1029/2004JB003174)
- Moss RES (2009) Reduced uncertainty of ground motion prediction equations through Bayesian variance analysis. Pacific earthquake engineering research (PEER) center, report 2009/105, November 2009
- Musson RMW, Sargreant SL (2007) Eurocode 8 seismic hazard zoning maps for the UK. Technical report CR/07/125, British Geological Survey, Keyworth, UK
- Petersen MD, Frankel AD, Harmsen SC, Mueller CS, Haller KM, Wheeler RL, Wesson RL, Zeng Y, Boyd OS, Perkins DM, Luco N, Field EH, Wills CJ, Rukstales KS (2008) Documentation for the 2008 update of the United States national seismic hazard maps. USGS open-file report 2008–1128, US Geological Survey, Reston, Virginia
- Power M, Chiou B, Abrahamson N, Bozorgnia Y, Shantz T, Roblee C (2008) An overview of the NGA project. *Earthq Spectra* 24:3–21
- Rey J, Faccioli E, Bommer J (2002) Derivation of design soil coefficient (S) and response spectral shapes for Eurocode 8 using the European Strong-Motion Database. *J Seismol* 6:547–555
- Rietbrock A, Strasser F, Edwards B (2013) A stochastic ground-motion prediction model for the UK. *Bull Seismol Soc Am* 103(1):57–77
- Sandikkaya MA, Akkar S (2012) How style-of-faulting ratios change with database features. *Seismol Res Lett* 83:123–124
- Sandikkaya MA, Akkar S, Bard P-Y (2013a) A nonlinear site amplification model for the new pan-European ground-motion prediction equations. *Bull Seismol Soc Am* 103:19–32
- Sandikkaya MA, Akkar S, Ay BÖ (2013b) Predictive models for horizontal and vertical conditional mean response spectra at multiple damping levels derived for Europe and the Middle East. *Bull Earthq Eng* (submitted to this issue)
- Scasserra G, Stewart JP, Bazzurro P, Lanzo G, Mollaioli F (2009) A comparison of NGA ground-motion prediction equations to Italian data. *Bull Seismol Soc Am* 99:2961–2978
- Scherbaum F, Cotton F, Smit P (2004) On the use of response spectral-reference data for the selection and ranking of ground-motion models for seismic-hazard analysis in regions of moderate seismicity: The case of rock motion. *Bull Seismol Soc Am* 94(6):2164–2185
- Scherbaum F, Cotton F, Staedtke H (2006) The estimation of minimum-misfit stochastic models from empirical ground-motion prediction equations. *Bull Seismol Soc Am* 96:427–445
- Scherbaum F, Delavaud E, Riggelsen C (2009) Model selection in seismic hazard analysis: an information-theoretic perspective. *Bull Seismol Soc Am* 99(6):3234–3247
- Scordilis EM (2006) Empirical global relations converting M_s and m_b to moment magnitude. *J Seismol* 10:225–236
- Spudich P, Joyner WB, Lindh AG, Boore DM, Margaris BM, Fletcher JB (1999) SEA99: a revised ground motion prediction relation for use in extensional tectonic regimes. *Bull Seismol Soc Am* 89:1156–1170
- Stafford PJ, Strasser FO, Bommer JJ (2008) An evaluation of the applicability of the NGA models to ground-motion prediction in the Euro-Mediterranean region. *Bull Earthq Eng* 6:149–177
- Strasser FO, Abrahamson NA, Bommer JJ (2009) Sigma: Issues, insights, and challenges. *Seismol Res Lett* 80:40–56
- Wells DL, Coppersmith KJ (1994) New empirical relationships among magnitude, rupture length, rupture width, rupture area, and surface displacement. *Bull Seismol Soc Am* 84:974–1002
- Westaway R, Smith RB (1989) Strong ground motion from normal-faulting earthquakes. *Geophys J* 96:529–559
- Yenier E, Sandikkaya MA, Akkar S (2010) Report on the fundamental features of the extended strong motion databank prepared for the SHARE project, pp. 44. Deliverable 4.1 of Seventh Framework Programme Project Seismic Hazard Harmonization in Europe (SHARE), 34 pages, Ankara
- Zhao JX, Zhang J, Asano A, Ohno Y, Oouchi T, Takahashi T, Ogawa H, Irikura K, Thio HK, Somerville PG, Fukushima Y (2006) Attenuation relations of strong ground motion in Japan using site classifications based on predominant period. *Bull Seismol Soc Am* 96:898–913